Comparative genomic and metabolic analysis of *Streptomyces* sp. RB110 morphotypes illuminates genomic rearrangements and formation of a new 46-membered antimicrobial macrolide

Soohyun Um,[a]‡ Huijuan Guo,[a]‡ Sirinthra Thiengmag,[b]‡ René Benndorf,[a] Robert Murphy,[c] Maja Rischer,[a] Daniel Braga,[b] Michael Poulsen,[c] Z. Wilhelm de Beer,[d] Gerald Lackner,[b*] and Christine Beemelmanns[a]*

a. Chemical Biology of Microbe-Host Interactions, Leibniz Institute for Natural Product Research and Infection Biology, Hans Knöll Institute (HKI), Beutenbergstraße 11a, 07745 Jena, Germany. E-mail: christine.beemelmanns@hki-jena.de
b. Synthetic Microbiology, Leibniz Institute for Natural Product Research and Infection Biology, Hans Knöll Institute (HKI), Beutenbergstraße 11a, 07745 Jena, Germany. E-mail: gerald.lackner@hki-jena.de
c. Section for Ecology and Evolution, Department of Biology, University of Copenhagen, Universitetsparken 15, 2100 Copenhagen East, Denmark.
d. Department of Biochemistry, Genetics, and Microbiology, Forestry and Agricultural Biotechnology Institute, University of Pretoria, Pretoria 0002, South Africa
‡ contributed equally.

Abstract

Morphotype switches frequently occur in Actinobacteria and are often associated with disparate natural product production. Here we report on differences in the secondary metabolomes of two morphotypes of a *Streptomyces* species, including the discovery of a novel antimicrobial glycosylated macrolide, which we named termidomycin A. While exhibiting an unusual 46-membered polyene backbone, termidomycin A (1) shares structural features with the clinically important antifungal agents amphotericin B and nystatin A1. Genomic analyses revealed a biosynthetic gene cluster encoding for a putative giant type I polyketide synthase (PKS), whose domain structure allowed us to propose the relative configuration of the 46-membered macrolide. The architecture of the biosynthetic gene cluster was different in both morphotypes, thus leading to diversification of the product spectrum. Given the high frequency of genomic rearrangements in Streptomycetes, the metabolic analysis of distinct morphotypes as exemplified in this study is a promising approach for the discovery of bioactive natural products and pathways of diversification.

Introduction

Social insects, such as bees, ants, and termites provide prime examples of divisions of labour, and extreme morphological differentiation allowing specialized functions within the colony.[1] Over the past 20 years, it has become evident that microbes engage in similar social behaviour. They exhibit characteristic phenotypic and metabolic features of coordinated labour divisions such as swarming or biofilm formation and require the secretion of public goods that are shared among their kin.[2-4] Amongst other bacterial lineages, *Streptomyces* have emerged as model organisms to analyse division of labour as they frequently become genetically heterogeneous because of amplifications and deletions to the chromosome,[5,6] which in turn may induce the irreversible genetic differentiation and division of labour within a single colony, causing, e.g., selective secondary metabolite production within subpopulations of cells of a colony.[7] While studying symbiotic Actinobacteria of the fungus-farming termite species *Macrotermes natalensis*,[8-10] which contribute to the protection of the monocultural fungal garden against co-occurring weed and parasitic fungi,[11-14] we observed that several isolated Actinobacteria showed morphological differentiation within a colony, exhibiting altered pigmentation and sporulation behaviour when cultivated in the laboratory.[15] Most notably, the parental isolate named *Streptomyces* sp. RB110 (Figure 1A), closely related to *Streptomyces californicus*, repeatedly showed the appearance of two distinct morphotypes, which we named RB110-1 and RB110-2 (Figure 1B). Based on the hypothesis that the observed morphological

differentiation might be caused by genomic rearrangements, we compared the genomes and metabolomes of both morphotypes. The comparative analysis resulted in the isolation of the novel antimicrobial polyketide termidomycin A (**1**) from morphotype RB110-2, which is structurally related to the clinically important antifungal agents amphotericin B and nystatin A1, the detection of a giant polyketide synthase as the putative biosynthetic origin of termidomycins and the detection of a genetic rearrangement in morphotype RB110-2, which is proposed to be the major cause of RB110-2 morphotype appearance and termidomycin A (**1**) production.

Results

Morphology. After its isolation from the termite-associated microbiome, *Streptomyces* sp. RB110-1 (parental strain) exhibited a morphological-distinct violet-coloured mycelium at the edges of each greenish-grey colony was observed (Figure 1A). The violet-coloured mycelium was aseptically transferred to new growth medium, which resulted in the propagation of a stable violet-coloured morphotype named RB110-2 (Fig 1B). While propagation of the greenish-grey parental morphotype repeatedly differentiated into RB110-2 when cultivated on different solid media, the reverse phenomenon was not observed. Subsequent studies of culture conditions revealed that morphotype RB110-1 showed strong sporulation after five to seven days of incubation. Only weak spore formation was observed for strain RB110-2 (Figure S1, S2). Similarly, strong differences in colony morphology/pigmentation between both strains were observed. While colonies of RB110-1 remained of greenish-grey appearance on MS agar, they adopted a violet-white colour on ISP1 and ISP2 media agar and remained of white colour on ISP3-ISP5. In contrast, colonies of RB110-2 appeared violet on MS agar, but were of white colour on ISP1 and revealed a red to violet pigment production on ISP2-ISP5 (Figure S25-S27).

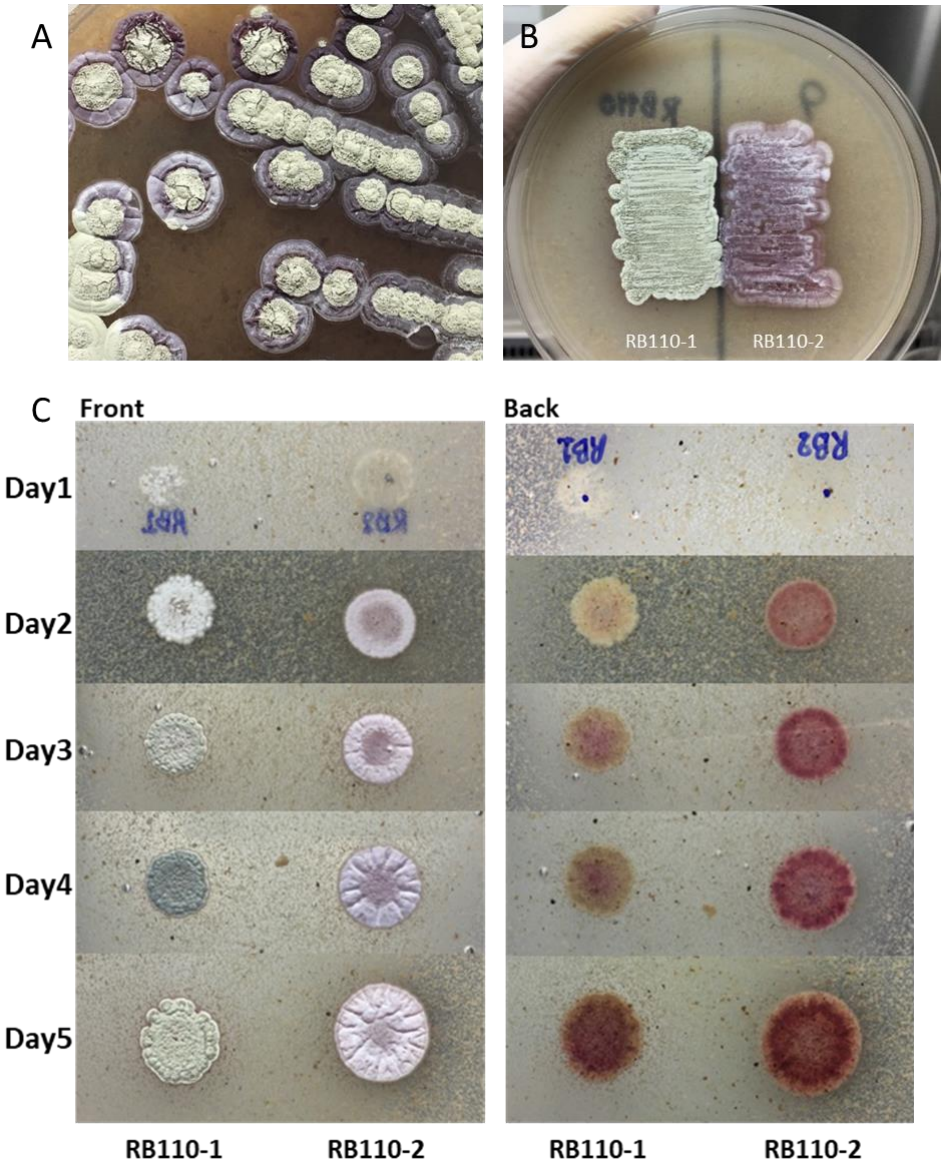

Figure 1. A) Colonies of a 14-day old *Streptomyces* sp. RB110 culture (MSA medium) showing two distinct morphologies (greyish-green and light-purple); B) cultures of both morphotypes (RB110-1 and RB110-2) after separation from parental strain and C) cultures grown on MS medium at 28 °C from 1-5 days (back and front side).

Genome sequencing. To exclude that RB110-2 was a contaminant of the parental culture, we sequenced the genomes of both morphotypes using Illumina and PacBio sequencing.[10] Both genomes were ~7.88 Mb long and with a G+C content of 72.5%, both typical values for *Streptomyces* species. Subsequent digital DNA-DNA hybridization (DDH)-based analysis finally proved that both variants of RB110 were highly related to each other (DDH values of 99.7-100%), thus excluding microbial contamination as the source of RB110-2. The DDH analysis and phylogenetic analysis based on the sequence alignment of the 16S rRNA gene further indicated that both morphotypes belong to the same species with *Streptomyces californicus* NBRC 12750T [DDH values of 81.0% (78.1-83.6%] being the closest relative (Figure S4, Table S7).[15] To investigate if large-scale genomic rearrangements might underlie the observed phenotype switch, a synteny plot was generated using Mummer 3.23 (Figure S3). Although a highly syntenic layout of both morphotype genomes was observed, a single transposition event was detectable. A region of 106.8 kb was transferred of from the start of the (linear) chromosome of RB110-1 to the end of the RB110-2 genome. Besides many hypothetical proteins, the transposed region indeed encoded for

genes annotated as transposase and enzymes involved in DNA binding and nucleic acid processing, such as helicases. However, neither a terminal inverted repeat region could be identified, nor any genes of structural phage components. Thus, it is possible that the rearrangement is rather a result of instability around the terminal regions of the linear chromosome than a specific excision/insertion event. At the current stage it is yet unclear if the genomic rearrangement or the accompanying metabolic changes account for the morphotype switch to *Streptomyces* sp. RB110-2 and further genetic and complementation studies will necessary to address these questions.

Metabolomic analysis. To evaluate if the difference in pigmentation of both morphotypes relates to changes in their antimicrobial properties, both strains were cultivated using the same growth conditions (mannitol soya (MS) or ISP2-mannitol (ISP*M) agar plates, Table S1) and metabolites were extracted with EtOAC. While extracts of RB110-1 showed good antibacterial activity against Gram-positive bacteria, the deep red-coloured extracts of RB110-2 revealed antibacterial activity as well as growth inhibitory activity against *Candida albicans* and *Penicillium notatum* (Table S4). To examine how the variations in pigmentation and bioactivities relate to metabolic differences of each morphotype, liquid chromatography/high-resolution tandem mass spectrometry (LC-HRMS^2) measurements in combination with Global Natural Product Social Molecular Networking (GNPS)[17] and dereplication analysis using Scifinder,[18] Antibase[19] and Compound Discoverer (Thermo Fisher) was performed on the obtained extracts. The MS-based analysis indicated a shared metabolome of RB110-1 and RB110-2 (Figure S5-S7), but also several distinct molecular ion clusters unique to either morphotype. Most intriguingly, RB110-2 extracts revealed an increased abundance of molecular features within the *m/z* range of 1250-1350 (Figure S5 and S6), several of which were yet unreported molecular ions. The dereplication approach allowed us to putatively assign some of the shared molecular ion clusters to compound families with reported antibacterial and antifungal properties, including the nonactin and griseorhodin families (Figure 2). While nonactins are 32-membered cyclic ionophore antibiotics originally isolated from *Streptomyces aureus,*[20] griseorhodins consist of highly oxygenated naphthoquinone and an isocoumarin moieties linked through a bis-benzannulated 6,5-spiroketal ring system.[21] Griseorhodins are of red color with a unique UV-Vis pattern and possess antibacterial and antifungal activities. Although both morphotypes appeared to produce griseorhodins and nonactins, morphological and metabolomic studies indicated an upregulated griseorhodin production in RB110-2, which was also visible by increased reddish pigmentation and detectable by an increased antimicrobial activity of the crude extract (Figure S7, Table S4).

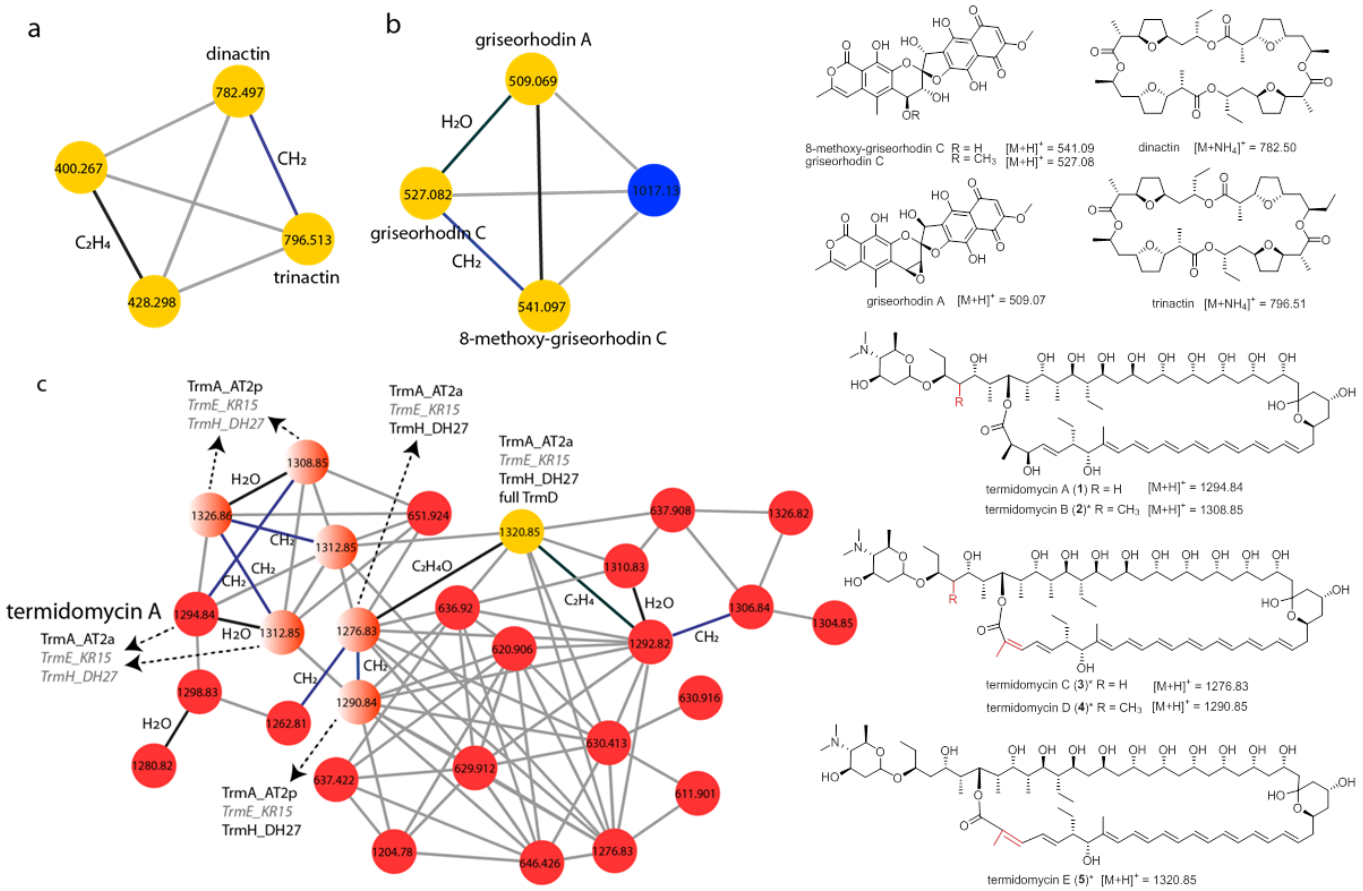

Figure 2. Section of HMRS^2-based GNPS network of *Streptomyces* sp. RB110-1 and *Streptomyces* sp. RB110-2 culture extracts (ISP2*M, 7 days, 30 °C, gold: RB110-1 and RB-110-2, blue: RB110-1; red: RB110-2): **a)** cluster assigned to dinactin and trinactin (*m/z* 782.497 and 796.513); **b)** cluster assigned to griseorhodins (*m/z* 509.069 and 541.097); and **c)** cluster assigned to termidomycin A (**1**, *m/z* [M+H]$^+$ 1294.83) and *in silico* predicted congeners assigned with an asterix (*putative structures). Yellow node with *m/z* [M+H]$^+$ 1320.85 is assigned to termidomycin E (**5**) derived from the biosynthetic assembly line with active (regular-black) and/or inactive (italic-grey) PKS-domains (Trm, *vide infra*). Oval nodes represent parent ions whose mass-to-charge ratios (*m/z*) [M+H]$^+$ are indicated as node labels. Connections between nodes indicate relatedness based on similarities between MS^2 spectra. The network was generated using 6 minimum matched ion fragments, a minimum cluster size of 2, and a cosine score of 0.8.

Purification and structure elucidation. To characterize the yet unreported molecular ion peaks (*m/z* 1250-1350), RB110-2 was cultivated on larger scale under static growth conditions [ISP2 medium supplemented with 2 g of mannitol per liter (ISP2*M), 500 plates (150x20 mm), 30 days, 30 °C], followed by extraction of mycelium covered agar plates with EtOAc. MS-guided purification of extracts by semi-preparative reverse-phase HPLC (phenyl-hexyl column) yielded one light- and acid-sensitive compound **1** (Figure S8-S12), which we named termidomycin A (**1**). Despite several purification and cultivation attempts, the isolation of additional termidomycin congeners as deduced from HRMS^2 data remained unsuccessful. The molecular formula of compound **1** was deduced by ESI-HRMS as $C_{70}H_{120}NO_{20}$ (*m/z* 1294.8397 [M+H]$^+$, calcd. 1294.8398) and the characteristic UV-Vis absorption maxima (λ_{max} 348, 363, and 387) pointed towards a polyene-type macrolide bearing several conjugated unsaturated aliphatic hydrocarbons (Figure S8). Due to the chemical instability of compound **1**, additional cultivation on ISP2 medium supplemented with 1-^{13}C acetate was performed to increase ^{13}C-NMR signal intensity to enable structure elucidation (Figure S14). The deduced molecular formula and the ^{1}H and ^{13}C NMR analyses indicated twelve degrees of unsaturation.

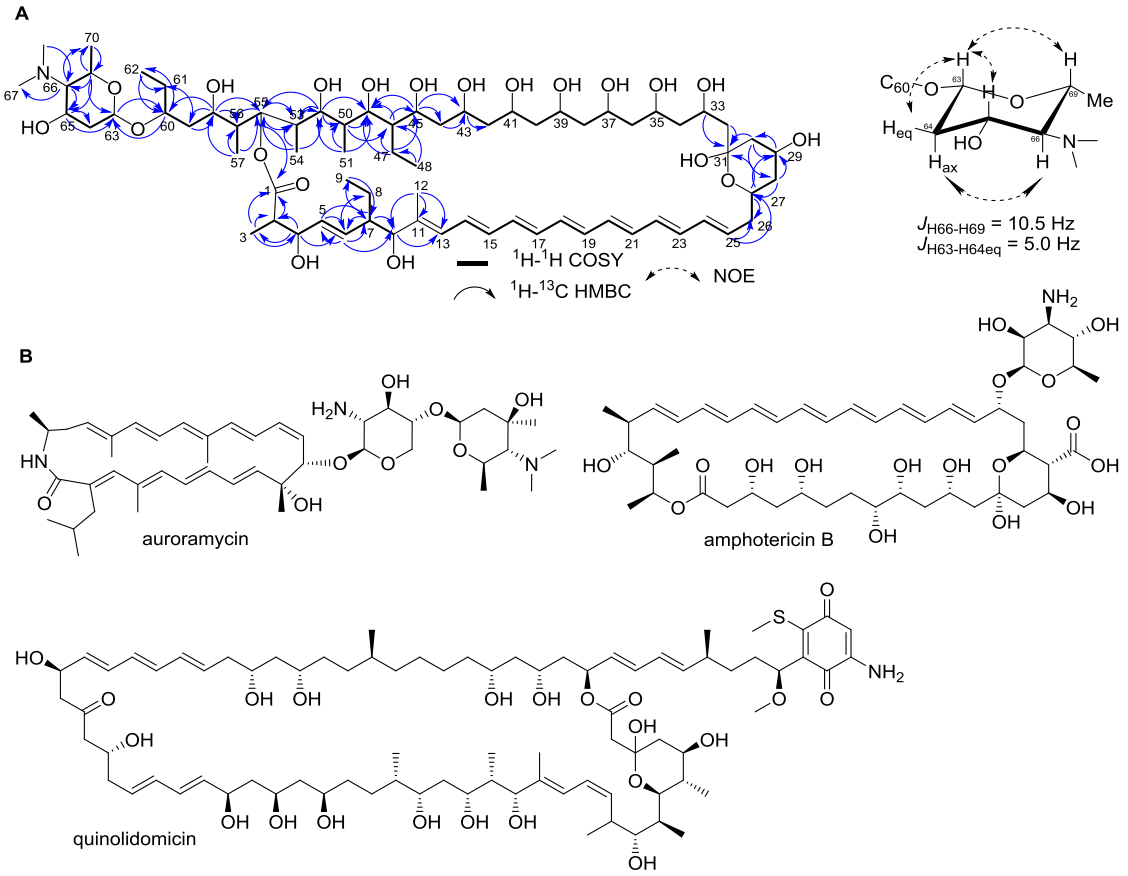

Figure 3. A) Planar structure of termidomycin A (**1**) showing observed COSY, HMBC correlation; NOESY correlation observed in the aminosugar D-kedarosamine. B) Chemical structures of related bioactive macrolides.

Detailed ^{13}C NMR analysis revealed 70 ^{13}C-signals, which correlated with the HRMS data, and included one ester carbon [δ_C 177.8] and 16 olefinic carbons [δ_C 143.1–127.5], which accounted for nine sites of the 12 degrees of unsaturation number and the presence of three rings (Table S2, Figure S28-S33). A detailed analysis of 1D (^{1}H and ^{13}C) and 2D NMR (HSQC, COSY, and HMBC) experiments in pyridine-d_5 confirmed that termidomycin A (**1**) consisted of 26 polyketide units carrying one aminoglycoside residue and a six-membered hemiketal ring (Table S2). This structural assumption was supported by MS^2 measurements that indicated e.g. the presence of an aminoglycoside moiety ($C_8H_{16}NO_2$, calcd. $[M+H]^+$ = 158.1176, Figure S8), and coupling constant analysis that indicated, e.g., a large vicinal-coupling constant between H-27 and H-28 [$J_{H27-H28}$ = 13.0 Hz] belonging to the hemiketal ring. HMBC correlations between the broad oxymethine proton [H-55, δ_H 6.11] and the ester carbonyl carbon [C-1; δ_C 177.8] allowed deducing the 46-membered macrolactone core structure, which satisfied the twelve degrees of unsaturation. While the overall relative stereochemistry for the heptaene group remained inconclusive due to the complexity of highly similar NMR patterns, the olefin configurations at C-5/C-6, C-13/C-14 and C-24/C25 were determined as *E* [J_{H5-H6} = 15.0 Hz, $J_{H13-H14}$ = 13.0 Hz, $J_{H14-H15}$ = 15.0 Hz, $J_{H24-H25}$ = 13.5 Hz] on the basis of NOE cross correlations and their coupling constants. Despite the instability of **1** towards light, heat, and chemical treatments, NMR analysis allowed to assign the aminoglycoside as kedarosamine by NOE analysis and Murata's method of *J*-based configurational assignment. The coupling between H-66 and H-69 ($J_{H66-H69}$ = 10.5 Hz) and strong NOESY correlations between H-63/H-64eq and H-63/H-69 indicated a *trans*-diaxial relation. Overall, the structure of compound **1** was deduced as a new 46-membered polyene macrolactone with a D-kedarosamine attached to C-60 by an *O*-glycosidic linkage as determined by HMBC correlation.

The polyene macrolide family includes antimicrobial nystatin A1 and amphotericin B, which are among the most important antifungal drugs (Figure 3B). Most derivatives are comprised of three up to seven double bonds in length, which are embedded within a 36-, 48-, 51- and

even 60-membered ring systems that most often contain a tetrahydropyran hemiketal ring within the macrolactone. While several 36-membered macrolides,[22,23] including antifungal liposidolides,[24] antiproliferative deplelides,[25] antifungal and cytotoxic astolides,[26] and caniferolides have been reported until today,[27] only very few examples exist for macrolides with larger ring sizes,2[8] such as the 48-membered monazomycin, the 51-membered stambomycins,[29] and the 60-membered macrolide named quinolidomicin A.[28,29] To the best of our knowledge a 46-membered macrolide containing a tetrahydropyran hemiketal ring, such as herein reported for termidomycin A, has not been reported yet. Most macrolides are glycosylated at specific hydroxyl positions, but the nature of the glycosyl moiety varies strongly. While stambomycins carry a *β*-mycaminose unit, amphotericin B is decorated with mycosamine. One of the closest structural homologs of the aminoglycoside kedarosamine of termidomycins is the aminoglycoside forosamine of auromycin.[30]

Biosynthetic pathway analysis. Subsequently, the genomes of RB110-1 and RB110-2 were analysed for the most-likely biosynthetic pathways using the AntiSMASH V5[31] and MIBiG platforms.[32] The polyene macrolide structure of compound **1** and ^{13}C-acetate labelling studies (Figure S14) already suggested a biosynthetic route involving a multi-modular type 1 polyketide synthase (PKS). Indeed, both genomes harboured only one candidate cluster region that encoded for a putative type 1 PKS and necessary decorating enzymes. The gene cluster region has a size of approx. 150 kb and encoded for about twenty biosynthesis-related genes, including eight type one PKS-related genes, a phosphopantetheinyl transferase (PPtase), a thioesterase, five genes related to glycosylation, a *N*-methyltransferase, a crotonyl-CoA carboxylase/reductase (Figure S17), a hydroxybutyryl-CoA dehydrogenase, one additional dehydrogenase as well as two transport-related proteins and two regulatory genes (Figure 4A, Table S8). To our surprise the alignment of both gene cluster regions revealed that both regions had an overall nucleotide sequence identity of almost 100%, except for a deletion of 4284 bp within the *trmD* gene in *trm-2* (RB110-2, Figure 4B). The break-points were contained in a repetitive region of 720 bp with both copies being 87% identical. On amino acid level the deletion resulted in the net loss of a complete PKS module (TrmD, M12/M13) with each of the recombination sites being part of the AT domains 12 and 13. (Figure 4B, Figure S15, S16). Since the module located between M11 and M14 represents a hybrid module of TrmD-1 M12 and M13, we denoted the new module present in TrmD-2 M12/13. Thus, the gene cluster regions were named *trm-1* (RB110-1) and *trm-2* (RB110-2), respectively.

***In silico* prediction of stereochemistry of termidomycin core structure**.

Due to the deduced structure of termidomycin A (**1**) and its origin RB110-2, gene cluster *trm-2* was deduced to be responsible for its production. Homology searches revealed that the PKS of *trm-2* was composed of a loading module (M1) and 26 extension modules (M2 to M27), equipped with a certain combination of acyl-carrier protein (ACP), acyltransferase (AT), dehydratase (DH), ketosynthase (KS), ketoreductase (KR), and enoyl reductase (ER) domains within each module.

Sequence analysis of the AT domains was in very good agreement with the identified structure of **1** (Figure S15, S16, S20-S23). While TrmC_AT6 and TrmH_AT25 were deduced to be responsible for the incorporation of ethylmalonyl-CoA, TrmA_AT1, TrmA_AT3, TrmB_AT4, TrmC_AT5, TrmG_AT24 and TrmH_AT27 were deduced to incorporate the necessary methylmalonyl-CoA units, with one exception (TrmA_AT2) as the deduced structure of termidomycin A (**1**) indicated that TrmA_AT2 might be able to incorporate both, malonyl-CoA as well as the predicted methylmalolyl-CoA. Subsequently, sequence alignment with known KR domains was carried out to propose the absolute stereochemistry of the chiral centres of the polyketide ring according to the model developed by Keatinge-Clay (Figure S17-S19, Table S9-S12);[33,34] an approach that has recently been employed to propose the absolute configuration of the 34-membered macrolides niphimycins,[35] 32-membered brasilinolides,[36] 36-membered macrolides caniferolides,[27] and the 60-membered macrocyclic quinolidomicin.[37,38] All KR domains were predicted to harbour a functional active site (Table S3, S9). Due to the absence of conserved LxD (LDD) motif in the loop region and the presence of tryptophan (W) and the absence of histidine (H) in the catalytic region 13 KRs (TrmA_KR2, KR3; TrmC_KR5, KR9, KR10; TrmD_KR11-KR14; TrmE_KR15-KR17; TrmH_KR25) were assigned as A1-type KRs. This led us to propose the stereochemistry on C-60, C-58, C-52, C-41, C-39, C-37, C-35, C-33, C-29, C-27, C-10 as '*R*' in the Keatinge-Clay '*RS*' system. The remaining KR domains were assigned as B1 type based on the presence of conserved LDD (or LED) motif in the loop region and the absence of

tryptophan (W) and YxP motif in the catalytic region, and the assignment of C-55, C-49, C-4 as the '*S*' configured according to the Keatinge-Clay '*RS*' system.

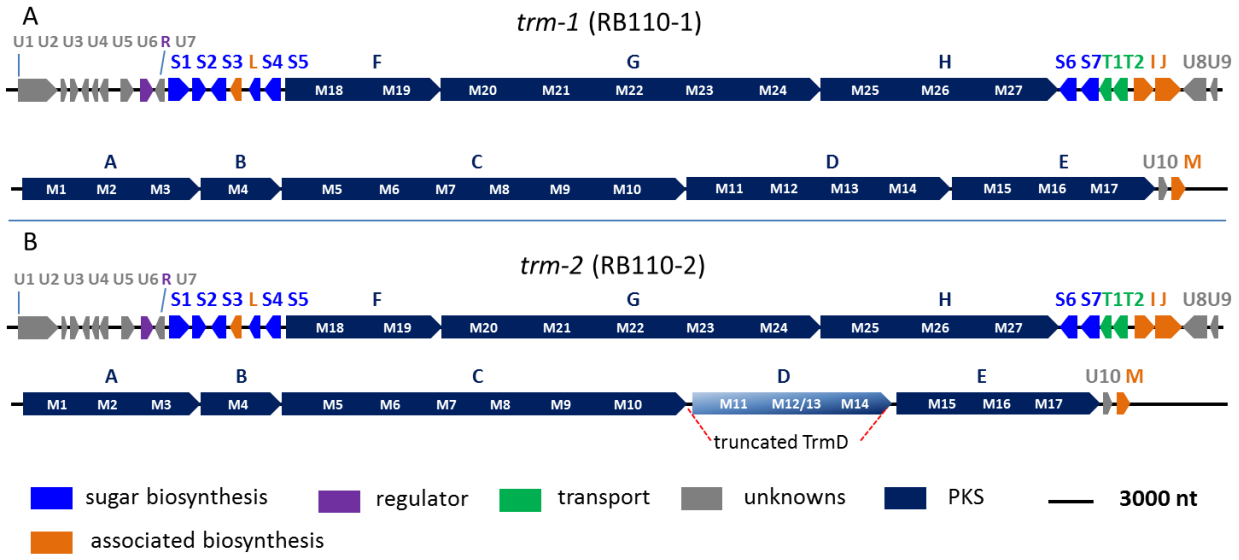

Figure 4. Schematic representation of the A) *trm-1* and B) *trm-2* gene cluster region. Sequence alignment revealed a deletion of a repetitive PKS region in *trm-2* between the AT domains of module 12 and 13 in Trm-2 resulting in a hybrid module M12/13 and a net loss of one PKS module (truncated TrmD in *trm-2*)

Although the module arrangement of *trm-2* and number of incorporated acetate/malonate units was in agreement with the core structure of **1**, the observed hemiketal formation (C-31) and hydroxylation pattern at C-4 and C-55 (atom numbering according to NMR assignment, Table S2) required one inactive KR domain (TrmE_KR15) and two dehydratases (TrmB_DH4 and TrmH_DH27) to be inactive or skipped during the assembly of the PKS core structure.[39] Sequence alignment of KR domains indicated that TrmE_KR15 harbours a functional active site, full-length analysis revealed an overall shorter amino acid sequence for TrmE_KR16 compared to other KR domains. Whether or not any of these findings is responsible for the dysfunctionality of the KR domain, remains speculative. Similarly, multiple sequence alignment of DH domains was performed to deduce the functionality of the DH-domains, but again all DHs were found to harbour the 'conserved' amino acid sequence and thus were predicted to have a functional active site.

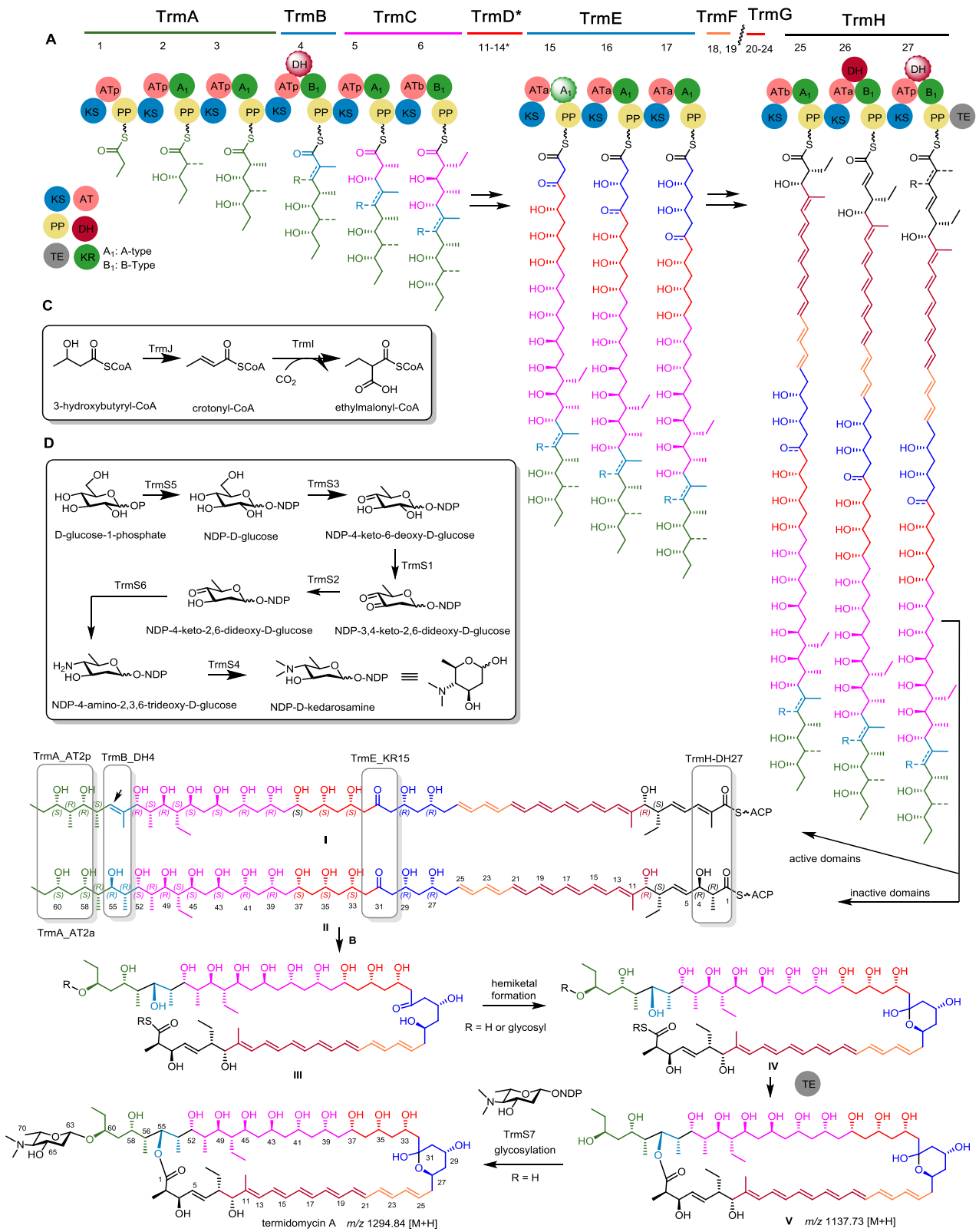

Figure 5 A) Proposed biosynthetic pathway (*truncated *trm-2* gene cluster) of the polyketide chain leading to the formation of core structure **I** (active domains) and core structure **II** (inactive domains) shown with predicted stereochemistry based on sequence alignment. (ATa: malonyl-CoA, ATp: methylmalonyl-CoA, ATb: ethylmalonyl-CoA, KRa: A-type ketoreductase, KRb: B-Type ketoreductase, with atom-numbering according to NMR assignment). B) Proposed sequence of modifying biosynthetic steps leading to termidomycin A (**1**). C-D) Putative biosynthesis of ethylmalonyl-CoA and aminosugar D-kedarosamine.

Glycosylation. Both *trm* gene clusters harbour identical genes that encode for the biosynthesis of NDP-D-kedorosamine and for a putative glycosyl transferase (TrmS7, 30% similar with SipS9) (Figure 5D). Here, it is important to note that NDP-D-kedorosamine shows high structural similarities to TDP-D-sipanose (sipanmycins)[40] and moderate similarity to NDP-L-kedarosamine (kedarcidin).[41] Homology searches revealed that *trm-2* encodes a putative glucose-1-phosphate thymidyltransferase (TrmS5, 69% similar with SipS7) and NDP-glucose 4,6-dehydratase (TrmS3, 76% similar with SipS6) that might be responsible for the biosynthesis of NDP-4-keto-6-deoxy-D-glucose from D-glucose-1-phosphate. Further dehydration catalysed by the putative NDP-hexose 2,3-dehydratase (TrmS1, 65% similar with SipS10) followed by reduction of the C-3 keto group of the putative NDP-hexose 3-ketoreductase TrmS2 (53% similar with SipS11) would lead to NDP-4-keto-2,6-dideoxy-D-glucose. Transamination could be catalysed by the putative aminotransferase (TrmS6, 74% similar with SipS13) leading to NDP-4-amino-2,3,6-trideoxy-D-glucose. The *N*-methylation is presumably catalysed by the putative N-methyltransferase (TrmS4, 81% similar with SipS8) generating NDP-D-kedarosamine. However, the timing and specificity of the glycosylation step remain unknown at this stage.

Structural congeners. As the detailed comparison of the *trm-1* and *trm-2* gene cluster revealed an almost identical arrangement and high homologies, except for the net loss of one module in TrmD (M12 and M13), the polyketide core structures of termidomycins produced by RB110-2 were predicted to be one CH_2CHOH group shorter compared to putative congeners of RB110-1. This, in addition to the small discrepancies observed between *in silico* predicted functionalities of single domains and the NMR-deduced structure of termidomycin, led us to perform an additional targeted $HRMS^2$-/GNPS-search for predicted congeners within culture extracts of both morphotypes (Figure 2, and Figures S20-S23). First, the acquired metabolic data of strain RB110-1 was searched for the absence/presence of the proposed longer-chain termidomycin congener E (**5**) (Figure 2C, Figure S20-S23), and indeed a fitting GNPS node with the *m/z* value 1320.8554 for $[M+H]^+$ was identified within the termidomycin cluster suggesting the active TrmH:DH27 domain and full TrmD modules. The low overall abundance of 1320.8554 $[M+H]^+$ correlated with notable lower metabolite production level (and pigmentation) in RB110-1 compared to RB110-2. A manual analysis of LC-MS^2 data of both strains revealed several molecular ion peaks within the termidomycin GNPS cluster, which were putatively assigned as congeners of termidomycin A (**1**) based on the molecular ion features and calculated chemical composition. While molecular ion peaks *m/z* $[M+H]^+$ 1308.8554 and 1326.8660 indicated the incorporation of methylmalonyl-CoA by the TrmA_AT domain, the *m/z* $[M+2H]^{2+}$ 638.9161 feature (node *m/z* 1276.83) suggested the production of a putative termidomycin C (**3**) derivative via an active TrmH_DH27. Similarly, the molecular ion *m/z* $[M+2H]^{2+}$ 645.9244 (node *m/z* 1290.84) supported e.g. an active TrmH_DH27 and the incorporation of methylmanoly-CoA via the TrmA_AT domain which would result in a putative termidomycin D (4) derivative, while node *m/z* 1308.85 suggested the formation of termidomycin E (5).

Bioactivity studies. Despite the intrinsic instability and often high toxicity of polyene macrolactams, several derivatives are world-leading drugs in clinical, use such as nystatin (tetraenes),[42] filipins (pentaenes)[43,44] and amphotericin B (heptaene).[44,45] As the numbers of conjugated double bonds within the polyene macrolides has been presumed to correlate with higher fungicidal activity, we anticipated a similar degree of antibiotic activity of termidomycin A (**1**). Indeed, activity studies revealed moderate to good antimicrobial activity against Gram-positive, Gram-negative bacteria and fungi (*Bacillus subtilis*, *Escherichia coli*, *Pseudomonas aeruginosa*, *Mycobacterium vaccae*, *Sporobolomyces salmonicolor* and *Penicillium notatum* (Table S5)) in comparison to the positive controls' ciprofloxacin and amphotericin B. Furthermore, first cell-based activity assays indicated that termidomycin A (**1**) exhibited also low cytotoxicity (HUVEC, K-562, and HeLa, >5 µg/mL of GI_{50} and GC_{50}, Table S6 and Fig S24).

Discussion

In this study, we observed a remarkable irreversible morphotype switch in *Streptomyces* sp. RB110, a phenomenon that has been proposed to allow for the division of labour amongst the bacterial population. The altered metabolic productivity[44] is believed to influence the population-wide fitness as well as interaction mechanisms with co-occurring microbes.[46-48] While the parental morphotype RB110-1 is more prolific in terms of spore formation, its emerging morphotype RB110-2 unleashes the production of additional antifungal metabolites, including the increased production of several griseorhodin derivatives and a novel 46-membered glycosylated macrolide named termidomycin A. Thus, it is hypothesized that the co-production of both antibiotics potentially offers a growth benefit or protection for the emerging genetically-heterogeneous bacterial colony and/or the spore-forming parental phenotype.[3,4]

The process of phenotypic differentiation of Actinobacteria, and *Streptomyces* in particular, is often a result of unexplained high-frequency rearrangements and deletions in their chromosome that cause the irreversible differentiation into genetically heterogeneous colonies.[3-5] Indeed, a chromosomal rearrangement was detectable in the emerging morphotype RB110-2 and is proposed to be directly or indirectly responsible for some of the observed morphological and metabolic changes connected to the switching event. Genome analysis also revealed the biosynthetic origin of the newly identified macrolide and comparison of the original BGC in RB110-1 (*trm-1*) and the homologous sequence in RB110-2 (*trm-2*) revealed a deletion in a highly repetitive PKS region encoded in *trm-2*, which justified the structural assignment of the isolated termidomycin A. Furthermore, subsequent i*n silico* studies of single domains of the *trm* gene cluster revealed the most likely absolute stereochemistry of the termidomycin core structure. From a drug-discovery perspective, our study highlights as one of the first examples that the systematic exploitation of a morphotype switch provides a unique strategy to discover novel natural products and allows unravelling the metabolic potential of Actinobacteria and putative natural functions of secondary metabolites; both aspects will attract more attention on this fascinating aspect of actinobacterial biology.

Author Contributions

SU: Data curation, Formal Analysis, Visualization, Writing – original draft, HG: Data curation, Formal Analysis, Visualization, Writing – original draft, review & editing, Validation, ST: Data curation, Formal Analysis, Visualization, Writing – review & editing, RB: Data curation, Formal Analysis, Visualization; RM: Data curation, Formal Analysis, MR: Data curation, Formal Analysis, DB: Data curation, Formal Analysis, MP: Resources, Supervision, Funding acquisition, Writing – review & editing, ZWB: Supervision, Funding acquisition, Writing – review & editing, GL: Conceptualization, Resources, Supervision, Funding acquisition, Writing – original draft and review & editing, Validation, CB: Conceptualization, Resources, Supervision, Funding acquisition, Writing – original draft and review & editing, Visualization

Conflicts of interest

There are no conflicts to declare.

Acknowledgements

This work was supported by the Deutsche Forschungsgemeinschaft (DFG, German Research Foundation) - CRC 1127/2 ChemBioSys – project ID 239748522 and BE 4799/3-1 to C. Beemelmanns. S. Um thanks the Humboldt Foundation for a postdoctoral fellowship and S. Thiengmag, D. Braga and G. Lackner thank the Carl Zeiss

Foundation for funding. R. Murphy and M. Poulsen are supported by a European Research Council Consolidator Grant (771349). We wish to thank H. Heinecke (Hans Knöll Institute, Jena) for measurement of NMR spectra, and C. Weigel (Hans Knöll Institute, Jena) and H.-M. Dahse (Hans Knöll Institute, Jena) for preliminary bioactivity studies.

Supporting Information

Supplementary Information (SI) is available free of charge and contains details on fermentation, cultivation, sample treatment, bioassays, isolation procedures, ESI-HRMS, ^{1}H NMR, ^{13}C NMR, and 2D NMR spectra as well as additional assay data.

General Experimental Procedures

Optical rotation was recorded using a P-1020 polarimeter (JASCO). IR spectrum was obtained on an FT/IR-4100 ATR spectrometer (JASCO). UV spectrum was acquired on a Shimadzu HPLC system. NMR experiments were carried out on a Bruker AVANCE III 600 MHz spectrometer, equipped with a Bruker Cryoplatform. The chemical shifts are reported in parts per million (ppm) relative to the solvent residual peak of pyridine-d_5 (^{1}H: 7.19, 7.55, 8.71 ppm; ^{13}C: 123.5, 135.5, 149.5 ppm). Semi-preparative HPLC was performed on a Shimadzu HPLC system using a phenyl-hexyl column C18(2) 250 x 10 mm column (particle size 10 µm, pore diameter 100 Å). Low resolution LCMS measurements were performed on a Shimadzu LCMS-2020 system equipped with single quadrupole mass spectrometer using a Phenomenex Kinetex C18 column (50 x 2.1 mm, particle size 1.7 µm, pore diameter 100 Å). Column oven was set to 40 °C; scan range of MS was set to *m/z* 150 to 2,000 with a scan speed of 10,000 u/s and event time of 0.25s under positive and negative mode. UHPLC-HESI-HRMS measurement was performed on a Dionex Ultimate3000 system combined with a Q-Exactive Plus mass spectrometer (Thermo Scientific) with a heated electrospray ion source (HESI). *Streptomyces* extracts were chromatographed in a Luna Omega C18 column (100 x 2.1 mm, particle size 1.6 µm, pore diameter 100 Å, Phenomenex) assembled with a SecurityGuard™ ULTRA guard cartridge (2 x 2.1 mm, Phenomenex). The column was held at 40 °C and with a flow rate of 300 µl/min. Chemicals: Methanol (VWR, Germany); water for analytical and preparative HPLC (Millipore, Germany); formic acid (Carl Roth, Germany); acetonitrile (VWR as LC-MS grade); media ingredients (Carl Roth, Germany). All the experiments were performed at Leibniz Institute for Natural Product Research and Infection Biology – Hans Knöll Institute, Jena, Germany.

Cultivation of parental strain: *Streptomyces* sp. RB110 was cultivated on solid medium (4 g of yeast extract, 10 g of malt extract, 4 g of glucose, and 18 g of agar per 1 L of sterilized water) at 25 °C. The bacterium was transferred to liquid 50 mL ISP2 broth in a 100-mL Erlenmeyer flask and cultivated at 30 °C at 180 rpm. After incubation for 7 days, 1 mL of the liquid culture was inoculated to each modified ISP medium 2 agar plate (4.0 g/L yeast extract, 5.0 g/L malt extract, 4.0 g/L soytone, 10.0 g/L glucose, 1 g/L mannitol, 20.0 g/L agar, 150 x20 mm, 40 0ea). The culture was cultivated at 30 °C in a dark condition to prevent from compound degradation for 6 days. The entire culture was extracted twice with 20 L of EtOAc overnight at 4 °C and the organic phase was concentrated *in vacuo*.

Cultivation of morphotypes: *Streptomyces* sp. RB110-1 and RB110-2 were cultivated on TSB at 30 °C for seven days (preculture) and then incubated on ISP media (ISP1-ISP5 using a 6 well-plate assay) using 50 µl of preculture for 18 days (Figure S1-S3). Time and media dependent analysis showed that there are indeed consistent differences between the two morphotypes, which differed in sporulation rate and colony morphology. For morphotype RB110-1 sporulation occurred after five days of incubation while no or only weak production of spores was observed for strain RB110-2 on ISP3, ISP4 and ISP5 even after five days (Figure S2). Colonies of RB110-1 had a violet-white color on ISP1, a light red color on ISP2 and a white color on ISP3-ISP5. Colonies of RB110-2 were of white color on ISP1 and revealed a red to violet pigment production on ISP2-ISP5.

DNA extraction: *Streptomyces* sp. RB110-1 and RB110-2 were grown in nutrient-rich ISP2 broth for 3 to 5 days at 30 °C (180 rpm) and cells were harvested after incubation by centrifugation for 10 min at 8000 x g. Genomic DNA was first extracted using the GenJet Genomic DNA Purification Kit (Thermo Scientific, #K0721) following the manufacture instructions with two slight changes (lysozym incubation time 40 min, protein kinase K treatment 40 min). DNA was quantified photometrically using a Nanodrop Lite Spectrometer (Thermo Scientific) photometer. High molecular weight DNA for PACBIO based whole genome sequencing was extracted using NucleoBond HMW DNA kit (Macherey-Nagel). Genomes are deposited at NCBI under the accession numbers RB110-1: JAEKDS000000000.1 and RB110-2: JAEKDR000000000.1.[10]

DNA-DNA hybridization (DDH): DNA-DNA hybridization was performed *in silico* at the GGDC web server with closest neighbour *Streptomyces californicus* NBRC12750.[48] Genome sequence of *Streptomyces californicus* NBRC12750 was downloaded from NCBI database (JNXW00000000.1).

Synteny plot: All genome contigs resulting from sequencing of the RB110-1 and RB110-2 morphotypes were used for a computation of syntenic regions (regions of conserved gene order) using Mummer 3.23.[49] While RB110-1 contigs were used as reference sequence, the contigs originating from RB110-2 served as query sequence. Visualization of synteny was performed using Mummerplot and Gnuplot (Figure S3).

Cultivation and extraction for GNPS-based analysis: Bacterial strains were cultured in 20 mL ISP2 medium. After incubation at 30 °C (180 rpm) for 7 days, the cultures were used to inoculate ISP2*M agar plates (1 mL culture was used for 150 x 20 mm plate, 3 plates) and ISP2*M liquid culture (1 mL culture was used for 100 mL broth), which were incubated at 30 °C for 7 days. The liquid culture was extracted with ethyl acetate (2 x 100 mL) using a separation funnel. The organic phase was concentrated *in vacuo* and analyzed by LC-MS^2. The mycelium covered culture was cut into small pieces, soaked with ethyl acetate (200 mL) overnight, filtered and ethyl acetate extract was dried under vacuum. The crude extract was dissolved with methanol, centrifuged for 10 min and then analyzed by LC-MS^2 (Figure S5-S10).

Large scale fermentation and purification: Strain RB110-2 was cultured on ISP2 medium at 28 °C and used to inoculate 200 mL ISP2*M liquid medium. After five days of incubation (30 °C at 180 rpm), 1 mL of the culture was used to inoculate ISP2 agar medium (500 plates, 150 x 20 mm) containing 0.2 mg of 1-^{13}C sodium acetate per liter to maximize the carbon chemical signals for ^{13}C NMR spectrum. All subsequent experiments were performed in the dark to avoid light-induced decomposition. After 7 days of cultivation at 30 °C in a dark incubator, plate cultures were cut into small pieces (50 x 50 mm) and extracted twice with 20 L of EtOAc overnight. The EtOAc layer was dried over Na_2SO_4 and concentrated *in vacuo* to yield 15.5 g of extract. To obtain pure termidomycin A (**1**), the dried substance was purified by semi-preparative reversed-phase HPLC on a phenyl-hexyl column (10 µm, 250 × 10 mm, a gradient solvent system; flow rate: 2 mL/min, detection: UV 383 nm, 20 to 50 % aqueous acetonitrile with 0.1 % F.A over 30 min) without an SPE fraction procedure to prevent from compound decomposition. Termidomycin A (**1**) eluted at 26 min (Figure S11-S14).

Physicochemical Data

Termidomycin A (**1**): yellow solid; $[\alpha]^{25}_{D}$ -42.0 (c 0.1 w/v%, MeOH); UV (MeOH) λ_{max} 348, 363, 387 nm; IR (ATR) ν_{max} 3399, 2610, 2360, 1741, 1581, 1460, 1425, 1387, 1263, 1194, 1099, 1023, 956, 913, 862, 774; NMR spectral data, see Table**1**; ESI-HRMS $[M + H]^+$ *m/z* 1294.8397 (calcd for $C_{70}H_{120}N_1O_{20}$, 1294.8398). For NMR analysis see, Table S2.

Notes and references

1. Gordon, D. M. (2016) From division of labor to the collective behavior of social insects, *Behav*. *Ecol*. *Sociobiol*. *70*, 1101–1108.
2. van Gestel, J., Vlamakis, H., and Kolter, R. (2015) Division of labor in biofilms: The ecology of cell differentiation, *Microbiol*. *Spectr*. *3*, 1–24.
3. West, S. A., and Cooper, G. A. (2016) Division of labour in microorganisms: An evolutionary perspective, *Nat*. *Rev*. *Microbiol*. *14*, 716–723.
4. Zhang, Z., Claessen, D., and Rozen, D. E. (2016) Understanding microbial divisions of labor, *Front*. *Microbiol*. *7*, 2070.
5. Barka, E. A., Vatsa, P., Sanchez, L., Gaveau-Vaillant, N., Jacquard, C., Meier-Kolthoff, J. P., Klenk, H. P., Clément, C., Ouhdouch, Y., and van Wezel, G. P. (2015) Taxonomy, physiology, and natural products of Actinobacteria, *Microbiol*. *Mol*. *Biol*. *Rev*. *80*, 1–43.

6. Volff, J. N., and Altenbuchner, J. (1998) Genetic instability of the *Streptomyces* chromosome, *Mol*. *Microbiol*. *27*, 239–246.
7. Zhang, Z., Du, C., de Barsy, F., Liem, M., Liakopoulos, A., Choi, Y. H., Claessen, D., and Rozen, D. E. (2020) Antibiotic production in *Streptomyces* is organized by a division of labor through terminal genomic differentiation, *Sci*. *Adv*. *6*, E5781.
8. Benndorf, R., Guo, H., Sommerwerk, E., Weigel, C., Garcia-Altares, M., Martin, K., Hu, H., Kuefner, M., de Beer, Z. W., Poulsen, M., and Beemelmanns, C. (2018) Natural products from Actinobacteria associated with fungus-growing termites, *Antibiotics 7*, E83.
9. Benndorf, R., Martin, K., Küfner, M., De Beer, Z. W., Vollmers, J., Kaster, A. K., and Beemelmanns, C (2020) *Actinomadura rubteroloni* sp. nov. and *Actinomadura macrotermitis* sp. nov., isolated from the gut of the fungus growing-termite *Macrotermes natalensis*, *Int. J. Syst. Evol. Microbiol*. *70*, 5255–5262.
10. Murphy, R., Benndorf, R., de Beer, Z. W., Vollmers, J., Kaster, A. K., Beemelmanns, C., and Poulsen, M. (2021) Comparative genomics reveals prophylactic and catabolic capabilities of *Actinobacteria* within the fungus-farming termite symbiosis, *mSphere 6*, e01233-20.
11. Ramadhar, T. T., Beemelmanns, C., Currie, C. R., and Clardy, J. (2014) Bacterial symbionts in agricultural systems provide a strategic source for antibiotic discovery, *J*. *Antibiot*. *67*, 53–58.
12. van Arnam, E. B., Currie, C. R., and Clardy, J. (2018) Defense contracts: molecular protection in insect-microbe symbioses, *Chem. Soc. Rev*. *47*, 1638–1651.
13. Otani, S., Challinor, V. L., Kreuzenbeck, N. B., Kildgaard, S., Christensen, S. K., Larsen, L. L. M., Aanen, D. K., Rasmussen, S. A., Beemelmanns, C., and Poulsen, M. (2019) Disease-free monoculture farming by fungus-growing termites, *Sci*. *Rep*. *9*, 1–10.
14. Scherlach, K., and Hertweck, C. (2018) Mediators of mutualistic microbe-microbe interactions, *Nat. Prod. Rep*. *35*, 303–308
15. Flärdh, K. and Buttner, M. J. (2009) *Streptomyces* morphogenetics: Dissecting differentiation in a filamentous bacterium, *Nat. Rev. Microbiol. 7*, 36–49.
16. Wayne, L. G., Brenner, D. J., Colwell, R. R., Grimont, P. A. D., Kandler, O., Krichevsky, M. I., Moore, L. H., Moore, W. E. C., Murray, R. G. E., Stackebrandt, E., Starr, M. P., and Trüper, H. G. (1987) Report of the ad hoc committee on reconciliation of approaches to bacterial systematics, *Int. J. Syst. Evol. Microbiol*. 37, 463–464.
17. Wang, M., Carver, J. J., Phelan, V. V., Sanchez, L. M., Garg, N., Peng, Y., Nguyen, D. D., Watrous, J., Kapono, C. A., Luzzatto-Knaan, T., Porto, C., Bouslimani, A., Melnik, A. V., Meehan, M. J., Liu, W. T., Crüsemann, M., Boudreau, P. D., Esquenazi, E., Sandoval-Calderón, M., Kersten, R. D., Pace, L. A., Quinn, R. A., Duncan, K. R, Hsu, C. C., Floros, D. J., Gavilan, R. G., Kleigrewe, K., Northen, T., Dutton, R. J., Parrot, D., Carlson, E. E., Aigle, B., Michelsen, C. F., Jelsbak, L., Sohlenkamp, C., Pevzner, P., Edlund, A., McLean, J., Piel, J., Murphy, B. T., Gerwick, L., Liaw, C. C., Yang, Y. L., Humpf, H. U., Maansson, M., Keyzers, R. A., Sims, A. C., Johnson, A. R., Sidebottom, A. M., Sedio, B. E., Klitgaard, A., Larson, C. B., Boya P, C. A., Torres-Mendoza, D., Gonzalez, D. J., Silva, D. B., Marques, L. M., Demarque, D. P., Pociute, E., O'Neill, E. C., Briand, E., Helfrich, E. J. N., Granatosky, E. A., Glukhov, E., Ryffel, F., Houson, H., Mohimani, H., Kharbush, J. J., Zeng, Y., Vorholt, J. A., Kurita, K. L., Charusanti, P., McPhail, K. L., Nielsen, K. F., Vuong, L., Elfeki, M., Traxler, M. F., Engene, N., Koyama, N., Vining, O. B., Baric, R., Silva, R. R., Mascuch, S. J., Tomasi, S., Jenkins, S., Macherla, V., Hoffman, T., Agarwal, V., Williams, P. G., Dai, J., Neupane, R., Gurr, J., Rodríguez, A. M. C., Lamsa, A., Zhang, C., Dorrestein, K., Duggan, B. M., Almaliti, J., Allard, P. M., Phapale, P., Nothias, L. F., Alexandrov, T., Litaudon, M., Wolfender, J. L., Kyle, J. E., Metz, T. O., Peryea, T., Nguyen, D. T., VanLeer, D., Shinn, P., Jadhav, A., Müller, R., Waters, K. M., Shi, W., Liu, X., Zhang, L., Knight, R., Jensen, P. R., Palsson, B. O., Pogliano, K., Linington, R. G., Gutiérrez, M., Lopes, N. P., Gerwick, W. H., Moore, B. S., Dorrestein, P. C., and Bandeira, N. (2016) Sharing and community curation of mass spectrometry data with Global Natural Products Social Molecular Networking, *Nat*. *Biotechnol*. *34*, 828-837.
18. Schwall, K., and Zielenbach, K. (2000) SciFinder a new generation of research tool. *Chem*. *Innov*. 30, 45-50.
19. Laatsch, H. (2017) AntiBase: The Natural Compound Identifier. Wiley-VCH, p 220.
20. Brian, R., Kusche, A., Smith, A. E., McGuirl, M. A., and Priestley, N. D. (2009) The alternating pattern of stereochemistry in the nonactin macrocycle is required for antibacterial activity and efficient ion binding, *J. Am. Chem. Soc*. *131*, 17155–17165.
21. Sperry, J., Wilson, Z. E., Rathwell, D. C. K., and Brimble, M. A. (2010) Isolation, biological activity and synthesis of benzannulated spiroketalnatural products, *Nat. Prod. Rep*. *27*, 1117–1137.
22. van Arnam, E. B., Ruzzini, A. C., Sit, C. S., Horn, H., Pinto-Tomás, A. A., Currie, C. R., and Clardy, J. (2016) Selvamicin, an atypical antifungal polyene from two alternative genomic contexts, *Proc. Natl. Acad. Sci. U. S. A*. *113*, 12940–12945.
23. Kim, D.-G., Moon, K., Kim, S.-H., Park, S.-H., Park, S., Lee, S. K., Oh, K.-B., Shin, J., and Oh, D.-C. (2012) Bahamaolides A and B, antifungal polyene polyol macrolides from the marine Actinomycete *Streptomyces* sp., *J. Nat. Prod*. *75*, 959−967.
24. Kihara, T., Koshino, H., Yamaguchi, I., Isono, K., and Shin, Y. C. (1995) Liposidolide A, a new antifungal macrolide antibiotic, *J. Antibiot*. *48*, 1385−1387.
25. Takeuchi, T., Hatano, M., Umekita, M., Hayashi, C., Wada, S.-i., Nagayoshi, M., Sawa, R., Kubota, Y., Kawada, M., Igarashi, M., and M. Shibasaki, (2017) ATP depletion assay led to the isolation of new 36-membered polyol macrolides deplelides A and B from *Streptomyces* sp. MM581-NF15, *Org. Lett. 19*, 4207-4210.
26. Alferova, V. A., Novikov, R. A., Bychkova, O. P., Rogozhin, E. A., Shuvalov, M. V., Prokhorenko, I. A., Sadykova, V. S., Kulko, A. B., Dezhenkova, L. G., Stepashkina, E. A., Efremov, M. A., Sineva, O. N., Kudryakova, G. K., Peregudov, A. S., Solyev, P. N., Tkachev, Y. V., Fedorova, G. B., Terekhova, L. P., Tyurin, A. P., Trenin, A. S., and Korshun, V. A. (2018) Astolides A and B, antifungal and cytotoxic naphthoquinone-derived polyol macrolactones from *Streptomyces hygroscopicus*, *Tetrahedron 74*, 7442–7449.
27. Pérez-Victoria, I., Oves-Costales, D., Lacret, R., Martín, J., Sánchez-Hidalgo, M., Diaz, C., Cautain, B., Vicente, F., Genilloud, O., and Reyes, F. (2019) Structure elucidation and biosynthetic gene cluster analysis of

caniferolides A–D, new bioactive 36-membered macrolides from the marine-derived *Streptomyces caniferus* CA-271066, *Org. Biomol. Chem*. *17*, 2954–2971.
28. Sawa, R., Kubota, Y., Umekita, M., Hatano, M., Hayashi, C., and Igarashi, M. (2018) Quadoctomycin, a 48-membered macrolide antibiotic from *Streptomyces* sp. MM168-141F8, *J. Antibiot*. *71*, 91–96.
29. Laureti, L., Song, L., Huang, S., Corre, C., Leblond, P., Challis, G. L., and Aigle, B. (2011) Identification of a bioactive 51-membered macrolide complex by activation of a silent polyketide synthase in *Streptomyces ambofaciens, Proc. Natl. Acad. Sci. U. S. A*. *108*, 6258–6263.
30. Lim, Y. H., Wong, F. T., Yeo, W. L., Ching, K. C., Lim, Y. W., Heng, E., Chen, S., Tsai, D. J., Lauderdale, T. L., Shia, K. S., Ho, Y. S., Hoon, S., Ang, E. L., Zhang, M. M., and Zhao, H. (2018) Auroramycin: A potent antibiotic from *Streptomyces roseosporus* by CRISPR-Cas9 activation, *Chembiochem 19*, 1716–1719.
31. Blin, K., Shaw, S., Steinke, K., Villebro, R., Ziemert, N., Lee, S. Y., Medema, M. H., and Weber, T. (2019) antiSMASH 5.0: updates to the secondary metabolite genome mining pipeline, *Nucleic Acids Res*. *47*, W81–W87.
32. Kautsar, S. A., Blin, K., Shaw, S., Navarro-Muñoz, J. C., Terlouw, B. R., van der Hooft, J. J. J., van Santen, J. A., Tracanna, V., Suarez Duran, H. G., Pascal Andreu, V., Selem-Mojica, N., Alanjary, M., Robinson, S. L., Lund, G., Epstein, S. C., Sisto, A. C., Charkoudian, L. K., Collemare, J., Linington, R. G., Weber, T., and Medema, M. H. (2020) MIBiG 2.0: a repository for biosynthetic gene clusters of known function. *Nucleic Acids Res*. *48*, D454–D458.
33. Zheng, J., Taylor, C. A., Piasecki, S. K., and Keatinge-Clay, A. T. (2010) Structural and functional analysis of A-type ketoreductases from the amphotericin modular polyketide synthase, *Structure 18*, 913–922.
34. Keatinge-Clay, A. T. (2016) Stereocontrol within polyketide assembly lines. *Nat. Prod. Rep*. *33*, 141–149.
35. Hu, Y., Wang, M., Wu, C., Tan, Y., Li, J., Hao, X., Duan, Y., Guan, Y., Shang, X., Wang, Y., Xiao, C., and Gan, M. (2018) Identification and proposed relative and absolute configurations of niphimycins C-E from the marine-derived *Streptomyces* sp. IMB7-145 by genomic analysis, *J. Nat. Prod. 81*, 178–187.
36. Chiu, H. T., Weng, C.-P., Lin, Y-C., and Chen, K.-H. (2016) Target-specific identification and characterization of the putative gene cluster for brasilinolide biosynthesis revealing the mechanistic insights and combinatorial synthetic utility of 2-deoxy-l-fucose biosynthetic enzymes, *Org. Biomol. Chem*. *14*, 1988–2006.
37. Hayakawa, Y., Shin-ya, K., Furihata, K., and Seto, H. (1993) Structure of a novel 60-membered macrolide, quinolidomicin A1, *J. Am. Chem. Soc*. *115*, 3014–3015.
38. Hashimoto, T., Hashimoto, J., Kozone, I., Amagai, K., Kawahara, T., Takahashi, S., Ikeda, H., and Shin-ya, K. (2018) Biosynthesis of quinolidomicin, the largest known macrolide of terrestrial origin: Identification and heterologous expression of a biosynthetic gene cluster over 200 kb, *Org. Lett*. *20*, 7996–7999.
39. Bevitt, D. J., Cortes, J., Haydock S. F., and Leadlay, P. F. (1992) 6-Deoxyerythronolide-B synthase 2 from Saccharopolyspora erythraea. Cloning of the structural gene, sequence analysis and inferred domain structure of the multifunctional enzyme, *Eur. J. Biochem*. *204*, 39–49.
40. Malmierca, M. G., Pérez-Victoria, I., Martín, J., Reyes, F., Méndez, C., Salas, J. A., and Olano, C (2020) New sipanmycin analogues generated by combinatorial biosynthesis and mutasynthesis approaches relying on the substrate flexibility of key enzymes in the biosynthetic pathway, *Appl. Environ. Microbiol*. *86*, e02453-19.
41. Lohman, J. R., Huang, S.-X., Horsman, G. P., Dilfer, P. E., Huang, T., Chen, Wendt-Pienkowski, E., and Shen, B. (2013) Cloning and sequencing of the kedarcidin biosynthetic gene cluster from *Streptoalloteichus* sp. ATCC 53650 revealing new insights into biosynthesis of the enediyne family of antitumor antibiotics, *Mol. Biosyst*. *9*, 478–491.
42. Ostrosky-Zeichner, L., Bazemore, S., Paetznick, V. L., Rodriguez, J. R., Chen, E., Wallace, T., Cossum, P., and Rex, J. H. (2001) Differential antifungal activity of isomeric forms of nystatin, *Antimicrob. Agents Chemother*. *45*, 2781–2786.
43. Djerassi, C., Ishikawa, M., Budzikiewicz, H., Shoolery, J. N., and Johnson, L. F. (1961) Terpenoids. XLVII. The structure of genipin, *Tetrahedron Lett*. *12*, 383–389.
44. Barreales, E. G., Rumbero, Á., Payero, T. D., de Pedro, A., Jambrina, E., and Aparicio, J. F. (2020) Structural and bioactivity characterization of filipin derivatives from engineered *Streptomyces filipinensis* strains reveals clues for reduced haemolytic action, *Antibiotics 9*, 413.
45. Cavassin, B. F., Baú-Carneiro, J. L., Vilas-Boas, R. R., and Queiroz-Telles, F. (2021) Sixty years of amphotericin B: An Overview of the main antifungal agent used to treat invasive fungal infections. *Infect. Dis. Ther*. ahead of print, doi: 10.1007/s40121-020-00382-7.
46. Molloy, E. M. and Hertweck, C. (2017) Antimicrobial discovery inspired by ecological interactions, *Curr. Opin. Microbiol. 39*, 121-127.
47. Adnani, N., Rajski, S. R., and Bugni, T. S. (2017) Symbiosis-inspired approaches to antibiotic discovery, *Nat. Prod. Rep*. *34*, 784–814.
48. Meier-Kolthoff, J. P., Auch, A. F., Klenk, H. P., and Goker, M. (2013) Genome sequence-based species delimitation with confidence intervals and improved distance functions, *BMC Bioinformatics 14*, 60.
49. Kurtz, S., Phillippy, A., Delcher, A. L., Smoot, M., Shumway, M., Antonescu, C., and Salzberg, S. L. (2004) Versatile and open software for comparing large genomes, *Genome Biol*. *5*, R12.